Bulletin of Earthquake Engineering
https://doi.org/10.1007/s10518-025-02189-8

ORIGINAL ARTICLE

A unified probabilistic assessment of multiple ground-motion intensity measures in seismic hazard analysis based on Fourier amplitude spectra

Haizhong Zhang[1] · Yan-Gang Zhao[2] · Rui Zhang[3] · Hongjun Si[4]

Received: 2 July 2024 / Accepted: 11 May 2025

Abstract
Different ground-motion intensity measures capture unique aspects of seismic motion, all of which play vital roles in probability seismic hazard analysis (PSHA), depending on the objectives under consideration and the design or analysis methods employed. Within the current PSHA framework, performing probability assessments for multiple intensity measures to obtain their seismic hazard curves typically requires multiple ground motion prediction equations (GMPEs) for each intensity measure. While GMPEs for some intensity measures can be approximated from existing ones through modifications, many still need to be developed through regression analyses of extensive earthquake data. However, besides the laborious task of constructing multiple GMPEs, recent studies have also pointed out the difficulty in directly constraining the scaling of these intensity measures within GMPEs using seismological theory. To address these challenges, this study proposes a more efficient, physically reasonable, and internally consistent framework for probabilistically analyzing multiple intensity measures. Firstly, to avoid the effort of constructing multiple GMPEs, this study exclusively adopts the GMPE of the Fourier amplitude spectrum (FAS) coupled with a ground-motion duration model. Subsequently, multiple intensity measures are simultaneously estimated based on theoretical relationships between FAS with each intensity measure. In addition, given that Fourier spectra are more closely related to the physics of wave propagation, the scaling of FAS in GMPE is easier to constrain using seismological theory. Furthermore, the moment method, in conjunction with Latin hypercube sampling, is applied to calculate the exceedance probability for each intensity measure, thereby obtaining corresponding seismic hazard curves. Finally, a numerical example was conducted to verify the proposed framework.

Keywords Multiple ground-motion intensity measures · Probabilistic seismic hazard analysis · Fourier amplitude spectrum · Moment method · Latin hypercube sampling

Extended author information available on the last page of the article

Published online: 13 June 2025

1 Introduction

Probabilistic seismic hazard analysis (PSHA) remains a useful tool to forecast the potentially destructive impact of earthquakes, thereby facilitating disaster prevention and mitigation efforts (Tselentis and Danciu 2010; Tselentis et al. 2010; Allen et al. 2020). An essential consideration in conducting PSHA involves selecting appropriate ground-motion intensity measures. Different intensity measures capture unique aspects of seismic motion, all of which play vital roles in PSHA, depending on the objectives under consideration and the design or analysis methods employed. The most commonly used intensity measures involve peak ground motions such as peak ground acceleration (PGA) and peak ground velocity (PGV), as well as pseudo-spectral acceleration (PSA). These measures offer simplicity and convenience in characterizing ground vibration, and their results derived from PSHA have found extensive use in seismic designs (AIJ 2015; ASCE/SEI 7–22 2022; Standards Australia 2007) as well as various other applications (Walker 2008; AIR-Worldwide 2013).

Nevertheless, these intensity measures each still have their limitations. Peak ground motions only capture the maximum amplitude value and fail to provide information on frequency content and duration of ground motion, while PSA incorporates frequency content but overlooks duration and cyclic loading effect of ground motion. In this regard, the input energy spectrum presents advantages as it integrates the amplitude, frequency content, and duration of ground motion (Kuwamura and Galambos 1989; Zhang et al. 2023a, b). The input energy spectrum, commonly expressed as the equivalent input energy velocity, V_{eq}, has also been utilized in PSHA (Chapman 1999; Tselentis et al. 2010; Zhang et al. 2024b) and has found application in energy-based seismic design (BSL 2005) in recent decades. Additionally, another intensity measure, Arias intensity, I_a, which is calculated as the integral of the square of the acceleration-time history, holds significant relevance in geotechnical domains (Reed and Kassawara 1990). Arias intensity I_a, reflecting the cumulative energy in seismic signals, demonstrates a strong correlation with Newmark's displacement and emerges as an effective intensity measure for assessing earthquake-induced landslide and liquefaction potential (Travasarou et al. 2003).

When aiming to generate seismic hazard curves and maps for these intensity measures to meet various applications, it is necessary to probabilistically analyze these intensity measures considering associated uncertainties in earthquakes. Within the current PSHA framework, this typically needs the following main components (Tselentis and Danciu 2010; Tselentis et al. 2010). Before conducting the analysis, all seismic faults/zones capable of producing damaging ground motions are identified, and their recurrence, magnitude, and distance distributions are evaluated. Then, the ground-motion prediction equations (GMPEs) for each intensity measure are selected to estimate these intensity measures at the sites of interest. Finally, seismic hazard curves for each intensity measure are calculated considering all the seismic faults/zones. It is noted that to probabilistically analyze multiple intensity measures and obtain their hazard curves, multiple GMPEs for each intensity measure are necessary. While GMPEs for some intensity measures can be approximated from existing ones through modifications, many still need to be developed via regression analyses of extensive earthquake data.

Although numerous GMPEs are available for some intensity measures like PGA and PSA in many regions worldwide (Douglas 2024), there is still a relatively limited number of GMPEs for other intensity measures in many regions, such as the equivalent input

energy velocity V_{eq} (Chapman 1999; Chou and Uang 2000; Cheng et al. 20142020; Alıcı and Sucuoğlu 20162018) and Arias intensity I_a (Travasarou et al. 2003). Additionally, since the characteristics of source, path, and site effects are systematically different in different regions, using GMPEs from other regions often leads to inaccurate estimations of ground motion (Bora et al. 2014; Lavrentiadis and Abrahamson 2023). Besides the efforts needed for constructing multiple GMPEs, there is another, more important challenge in developing GMPEs for multiple intensity measures. Bora et al. (2016) discovered that high-frequency PSA is influenced by a broad frequency range of ground motion and does not adhere to the linear system theory. Stafford et al. (2016) and Zhang and Zhao (2021b) further noted that site response for PSA is also nonlinear and depends on the frequency content of the input motion, even for linear soils (soil behavior at small strain). Therefore, many recent studies (Bora et al. 2014; Bayless and Abrahamson 2019) have emphasized the difficulty in directly constraining the scaling of PSA within GMPEs using seismological theory. Moreover Zhang et al. (2023b) found that site response for V_{eq} is also nonlinear and depends on the frequency content of the input motion, even for linear soils. Actually, the limitations of PSA are likely to extend to other intensity measures, including peak ground motions, equivalent input energy velocity V_{eq}, and Arias intensity I_a, due to their dependence on a broad frequency range of ground motion, as detailed in Section 3.

To address these challenges, this study proposes a more efficient, physically reasonable, and internally consistent framework for probabilistically analyzing multiple intensity measures. To avoid the laborious task of constructing multiple GMPEs, this study exclusively adopts the GMPE of Fourier amplitude spectrum (FAS) coupled with a ground-motion duration model. Subsequently, multiple intensity measures are simultaneously estimated based on theoretical relationships between FAS with each intensity measure. In addition, given that Fourier spectra are more closely related to the physics of wave propagation, the scaling of FAS in GMPEs is easier to constrain using seismological theory. Furthermore, the moment method, in conjunction with Latin hypercube sampling, is applied to calculate the exceedance probability for each intensity measure, thereby obtaining corresponding seismic hazard curves. The rest of the paper is organized as follows. Section 2 reviews the approach for probabilistically assessing multiple intensity measures in the current PSHA framework. Section 3 presents the approach for estimating multiple intensity measures from FAS, based on theoretical relationships between FAS and each intensity measure. Section 4 presents the approach for calculating the exceedance probability and seismic hazard curves for each intensity measure. Section 5 conducts a numerical example to verify the proposed framework. Lastly, Section 6 summarizes the conclusions.

2 Probabilistic assessment of multiple intensity measures in the current PSHA framework

This section briefly reviews the approach for probabilistically assessing multiple intensity measures and deriving their seismic hazard curves within the current PSHA framework. Before conducting the assessment, all seismic faults/zones capable of producing damaging ground motions are identified, and their recurrence, magnitude, and distance distributions are evaluated. Then, GMPEs for each intensity measure are selected to estimate these intensity measures at the sites of interest. Finally, the exceedance probabilities for multiple inten-

sity measures and their corresponding seismic hazard curves are calculated by considering all the seismic faults/zones. The probability that an intensity measure (IM) exceeds a specified intensity value, *im*, during a specified period *t* (years), *P*(IM>*im, t*), can be estimated by the following equation,

$$\mathrm{P}(\mathrm{IM} > im, t) = 1 - \prod_{k=1}^{m} [1 - \mathrm{P}_k(\mathrm{IM} > im,\ t)] \tag{1}$$

where, *k* refers to the *k*th earthquake originating from a seismic fault or seismic zone, *m* represents the number of seismic faults or zones considered capable of producing damaging ground motions, and P_k(IM>*im, t*) is the exceedance probability calculated only considering the *k*th earthquake. If the occurrence of seismic events is assumed to follow a homogenous stochastic Poisson process, P_k(IM>*im, t*) can be expressed as,

$$P_k(\mathrm{IM} > im, t) = 1 - e^{-p_k v_k t} \tag{2}$$

Here, v_k is the mean annual rate of the *k*th seismic fault or zone, p_k is the exceedance probability of the *k*th earthquake given the occurrence of the earthquake, which is expressed as,

$$p_k(\mathrm{IM} > im) = \int_R \int_M P\left(\mathrm{IM} > im \middle| m, r\right) f_M(m) f_R(r) dm dr \tag{3}$$

where, $f_M(m)$ represents the probability density function (PDF) of the magnitude occurring in the source; $f_R(r)$ is the PDF that describes the distribution of distance due to the spatial distribution of potential hypocenter locations within the seismic faults or zones. *P*(IM>*im*|*m, r*) is the probability that the intensity IM exceeds a specified value *im*, given a magnitude *m* and a distance *r*. *P*(IM>*im*|*m, r*) is commonly estimated using a GMPE, assuming that the natural logarithm of the IM for given a magnitude and a distance follows a normal distribution. Therefore, to calculate the probability *P*(IM>*im*|*m, r*) for multiple intensity measures, multiple GMPEs for each intensity measure are necessary. Figure 1 (a) depicts the schematic diagram for analyzing multiple intensity measures within the current PSHA framework.

3 Estimation of multiple intensity measures

3.1 Basic concept of the proposed framework

To avoid the laborious task of constructing multiple GMPEs, it would be ideal to use a single intensity measure that has dependent relationships with other intensity measures. Such that, the GMPE for only one intensity measure needs to be developed, and other intensity measures can be immediately obtained through their respective relationships. Additionally, deriving the desired intensity measures from a central GMPE ensures internal consistency among these intensity measures. Many previous studies (Boore 2003; Zhang and Zhao 20202021a2022; Zhang et al. 2023a, b; Zhao et al. 2023; Zhang et al. 2024a,

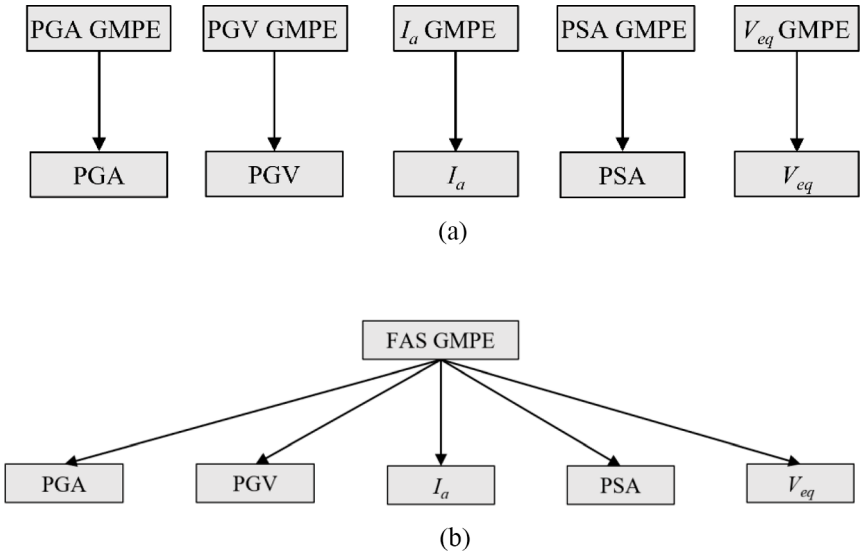

Fig. 1 Schematic diagrams of (**a**) the current PSHA framework and (**b**) the proposed framework for analyzing multiple intensity measures

b) have found that the FAS have dependent relationships with many intensity measures. In addition, regarding the difficulty in directly constraining the scaling of multiple intensity measures within GMPEs using seismological theory, many studies (e.g. Bora et al. 2014; Bayless and Abrahamson 2019) have highlighted that since Fourier spectra are more closely related to the physics of wave propagation, the scaling of FAS in GMPEs is easier to constrain using seismological theory. Therefore, this study exclusively adopts the GMPE of FAS coupled with a ground-motion duration model. Subsequently, multiple intensity measures are simultaneously estimated based on theoretical relationships between FAS with each intensity measure. Furthermore, the moment method, in conjunction with Latin hypercube sampling, is applied to calculate the exceedance probability for each intensity measure, thereby obtaining corresponding seismic hazard curves, which will be detailed in Section 4. Figure 1 (b) depicts the schematic diagram of the proposed framework for analyzing multiple intensity measures. The basic idea of the proposed framework can be clearly understood by comparing Fig. 1 (a) and 1 (b).

3.2 Multiple intensity measures from Fourier amplitude spectrum

Intensity measures including PGA, PGV, and PSA can be estimated from FAS based on random vibration theory (RVT) using the following equation (Boore 2003),

$$IM = pf\sqrt{\frac{1}{D\pi}\int_0^\infty |Y(\omega) \times I(\omega)|^2 d\omega} \tag{4}$$

where, ω is the circular frequency of the ground motion, $Y(\omega)$ is the acceleration FAS of the ground motion, pf represents the peak factor, and D represents the duration (details

presented subsequently). $I(\omega)$ is a filter that depends on the type of intensity measure being estimated. When Eq. (4) is applied to estimate the peak ground motions, the filter $I(\omega)$ is expressed as follows:

$$I(\omega) = \omega^n \tag{5}$$

where $n=0$ and -1 for PGA and PGV, respectively. When Eq. (4) is applied to estimate the PSA, the filter $I(\omega)$ is expressed as follows:

$$I(\omega) = \frac{1}{\sqrt{(2\xi\omega/\bar{\omega})^2+((\omega/\bar{\omega})^2-1)^2}} \tag{6}$$

where $\bar{\omega}$ and ξ are the circular frequency and damping ratio of the single-degree-of-freedom (SDOF) oscillator, respectively.

Many peak-factor models have been developed for RVT analyses (Cartwright and Longuet-Higgins 1956; Davenport 1964; Vanmarcke 1975). Although the Cartwright and Longuet-Higgins (CL) (1956) model has been commonly applied in engineering seismology and site response analyses, the Vanmarcke model (1975) can give better estimations of the peak factor (Wang and Rathje 2016). This is because the Vanmarcke model accounts for the dependence between peaks, which is particularly significant for the narrowband oscillator response, whereas the CL model does not. The cumulative distribution function (CDF) of the peak factor *pf* provided by Vanmarcke (1975) is expressed as follows:

$$P(pf < r) = [1-e^{(-r^2/2)}] \times exp[-2f_z e^{(-r^2/2)} D_{gm} \frac{(1-e^{-\delta^{1.2} r\sqrt{\pi/2}})}{(1-e^{r^2/2})}] \tag{7}$$

Here, D_{gm} represents the ground-motion duration, and δ is a bandwidth factor that is defined as a function of the spectral moments,

$$\delta = \sqrt{1-\frac{m_1^2}{m_0 m_2}} \tag{8}$$

where, m_0, m_1, and m_2 denote the zeroth-, first-, and second-order moments of the square of the FAS. It should be noted that the spectral moments should be calculated according to the intensity measures being estimated. To estimate the PGA and PGV, the FAS of acceleration and velocity of the ground motion should be used, respectively. To estimate PSA, oscillator-response FAS should be used accordingly. Therefore, the nth-order spectral moment, m_n, can be expressed as:

$$m_n = \frac{1}{\pi} \int_0^\infty \omega^n (Y(\omega) \times I(\omega))^2 d\omega \tag{9}$$

In addition, f_z denotes the rate of zero crossings that is also a function of the spectral moments, and is given by

$$f_z = \frac{1}{2\pi}\sqrt{\frac{m_2}{m_0}} \tag{10}$$

In RVT analyses, the expected value of *pf* is typically used. According to Eq. (7), the expected value of *pf* is calculated by $\int_0^\infty [1 - P(pf<r)]dr$.

The duration D also depends on the intensity measures being estimated. When Eq. (4) is applied to estimate the peak ground motions, D is equal to the ground-motion duration D_{gm}. When Eq. (4) is applied to estimate PSA, D is equal to the root-mean-square (rms) duration of the oscillator response, D_{rms}. Boore and Joyner (1984) and Liu and Pezeshk (1999) developed simple formulas to calculate the rms duration D_{rms} from D_{gm}. Boore and Thompson (2015) then developed a more accurate formula for D_{rms} as,

$$\frac{D_{rms}}{D_{gm}} = (c_{e1}+c_{e2}\frac{1-\eta^{c_{e3}}}{1+\eta^{c_{e3}}})[1+\frac{c_{e4}}{2\pi\xi}(\frac{\eta}{1+c_{e5}\eta^{c_{e6}}})^{c_{e7}}] \tag{11}$$

Here, $\eta = T_0/D_{gm}$, T_0 is the SDOF oscillator period, and c_{e1}–c_{e7} are coefficients that depend on the moment magnitude M and distance R, as noted in Boore and Thompson (2015).

In addition, Arias intensity I_a can be obtained from FAS by (Boore 2003),

$$I_a = \frac{\pi}{2g}m_0 \tag{12}$$

where g is gravitational acceleration and m_0 represents the zeroth-order moment of the square of the ground-motion acceleration FAS.

Moreover, the equivalent input energy velocity V_{eq} can be obtained from FAS by the following equation (Ordaz et al. 2003; Zhang et al. 2023a, b):

$$V_{eq}(\bar{\omega},\xi) = \sqrt{-\frac{2}{\pi}\int_0^\infty |Y(\omega)|^2 Re[Hv(\bar{\omega},\omega,\xi)]d\omega} \tag{13}$$

where $Hv(\bar{\omega},\omega,\xi)$ denotes the oscillator transfer function of the ground acceleration to the relative velocity, which is a complex number; its real part is expressed as:

$$Re[Hv(\bar{\omega},\omega,\xi)] = -\frac{2\xi\bar{\omega}\omega^2}{(\bar{\omega}^2-\omega^2)^2+(2\xi\omega\bar{\omega})^2} \tag{14}$$

Based on these equations, multiple intensity measures can be estimated from FAS. It is noted that to estimate PGA, PGV, and PSA from FAS, the ground motion duration D_{gm} is required. However, to estimate I_a and V_{eq} from FAS, D_{gm} is unnecessary. Additionally, similar to PSA, all these intensity measures, including PGA, PGV, I_a, and V_{eq}, are influenced by a broad frequency range of ground motion. This is because their calculations all involve the integral of FAS throughout the entire frequency domain. Therefore, it can be inferred that similar to PSA, all these intensity measures do not follow a linear system theory, and it is difficult to directly constrain the scaling of these intensity measures within GMPEs using seismological theory.

3.3 Comparison with time-series analysis

To demonstrate the accuracy of the equations presented in Section 3, the results for PGA, PGV, PSA, V_{eq}, and I_a, estimated from the FAS using these equations, were compared with those obtained through traditional time-series analysis. For this purpose, 118 real seismic ground accelerations were selected from K-NET and KiK-net in Japan. These seismic ground accelerations were recorded at 22 stations, covering four site classes (B, C, D, and E) as defined in the National Earthquake Hazards Reduction Program (NEHRP) (2000), based on the average shear-wave velocities in the upper 30 m, Vs_{30}. The magnitude M of these records varies from 4 to 8, and the distance R varies from 20 to 200 km.

The results of PGA, PGV, PSA, V_{eq}, and I_a were calculated from FAS of these seismic records using equations in Section 3 and compared with those obtained from time-series analysis. In the time-series analysis, PSA values were calculated using the direct-integration method by Nigam and Jennings (1969). Additionally, the values of V_{eq} were calculated based on the definition in the time-series domain,

$$V_{eq} = \sqrt{-2\int_0^{t_0} \ddot{x}_g \dot{x} dt} \tag{15}$$

where $\ddot{x}_g$ is the ground motion acceleration, $\dot{x}$ is the corresponding velocity response of the SDOF oscillator, t represents time, and t_0 is ground-motion duration corresponding to the end of the time series. In addition, the values of I_a were also calculated based on the definition in the time-series domain,

$$I_a = \frac{\pi}{2g}\int_0^{t_0} \ddot{x}_g^2 dt \tag{16}$$

Representative comparisons of PSA and V_{eq} for one station from each site class (a total of four stations) are shown in Figs. 2 and 3, respectively. Comparisons of PGA, PGV, and I_a for all seismic records across all stations are presented in Fig. 4. The ratios of the average PSA and V_{eq} values obtained from time-series analysis to those from Eqs. (4) and (13), considering all seismic records, are shown in Fig. 5. The results indicate that PSA, V_{eq}, PGA, PGV, and I_a obtained using the equations in Section 3 generally agree well with those obtained from time-series analysis, although the errors for PGA and PGV appear high for certain cases. The average relative errors across all cases are 16% for PSA, 2% for V_{eq}, 14% for PGA, 25% for PGV, and 1% for I_a.

Additionally, simulated FAS and time series were used to investigate the accuracy of the equations presented in Section 3. The FAS $Y(\omega)$ was generated based on a widely used point-source FAS model introduced by Boore (2003). The values of the seismological parameters required for this model were determined according to Boore and Thompson (2015), consistent with those used by Zhang et al. (2024b). The time series for the analysis were generated from the FAS using the Stochastic Method SIMulation (Boore 2005) program using stochastic simulations (Boore 1983). For each FAS, a suite of 100 time series signals was generated. Each time series signal exhibited distinct amplitude and phase characteristics in its Fourier spectrum, while the average FAS of the simulated time series matched the target FAS derived from the point-source model. The differences between each time series

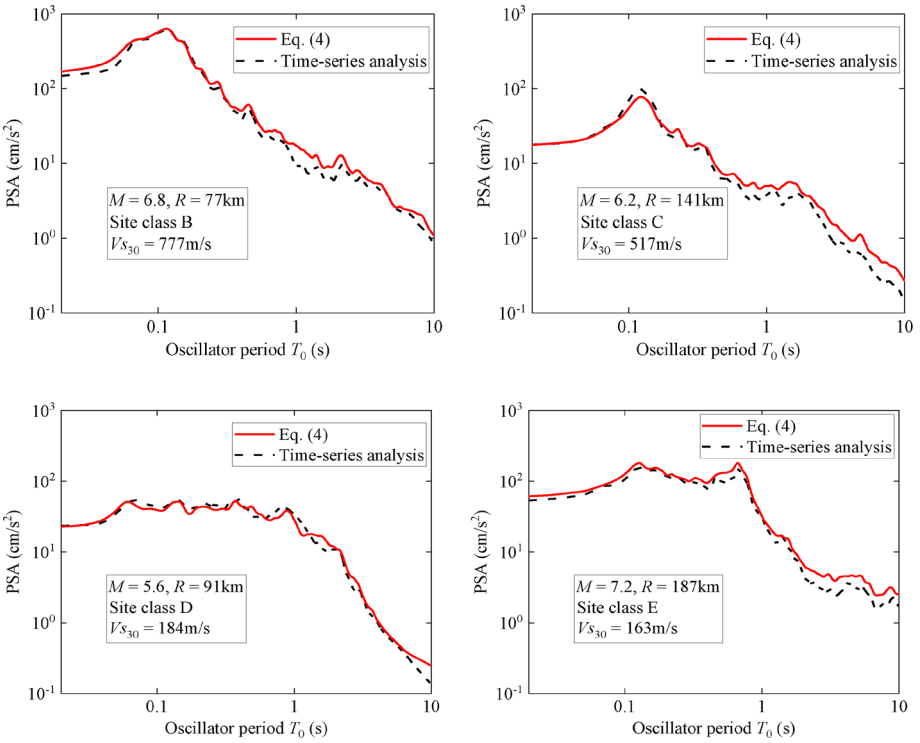

Fig. 2 Comparisons of PSA results calculated using Eq. (4) and time-series analysis based on real seismic records

signal arise from the band-limited white Gaussian noise incorporated into the simulation, as proposed by Boore (1983). A wide range of oscillator periods T_0 (0.02–10 s), moment magnitudes M (4–8), and distances R (20–200.01 km), were considered for the calculations. The selection of distance values also considers computational simplicity. Equation (11) for the rms duration D_{rms} requires coefficients c_{e1}–c_{e7}, which are provided for discrete distances (e.g., 50.24 km) by Boore and Thompson (2015). To avoid interpolation, the distances corresponding to these directly available coefficients are used. In addition, the oscillator damping ratio ξ is set to be 5%.

For each FAS, the 100 corresponding results of PGA, PGV, PSA, V_{eq}, and I_a were averaged and compared with those obtained using the equations presented in Section 3. Some of these representative comparisons are shown in Figs. 6, 7 and 8. Figure 6 shows the results of PSA, Fig. 7 shows the results of V_{eq}, and Fig. 8 shows the results of PGA, PGV, and I_a. In Fig. 8, each point represents a different combination of magnitude and distance, corresponding to the 20 scenarios shown in Figs. 6 and 7 for PSA and V_{eq}. The favorable agreement in these figures demonstrates the accuracy of the equations presented in Section 3. The average relative errors across all cases are 2% for PSA, 2% for V_{eq}, 7% for PGA, 6% for PGV, and 2% for I_a, which are consistent with those typically observed in previous studies (Boore 2003; Boore and Thompson 2015; Zhang and Zhao 2020; Zhang et al. 2024b). The largest errors in PSA occurred for the case with M=8 and R=20 km, with the average rela-

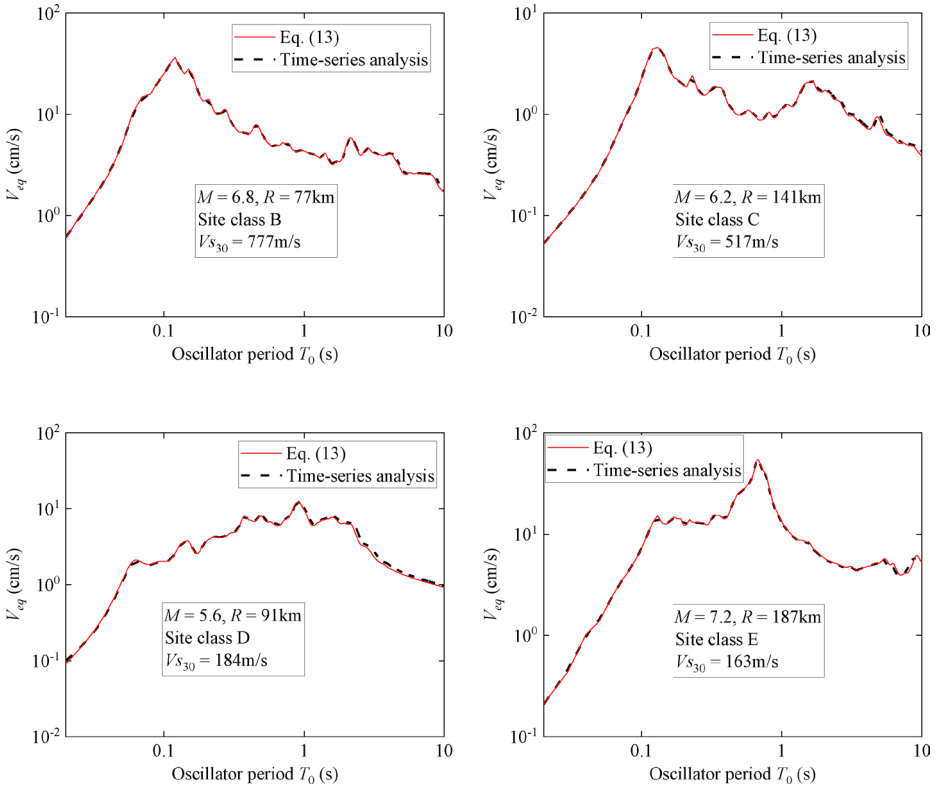

Fig. 3 Comparisons of V_{eq} results calculated using Eq. (13) and time-series analysis based on real seismic records

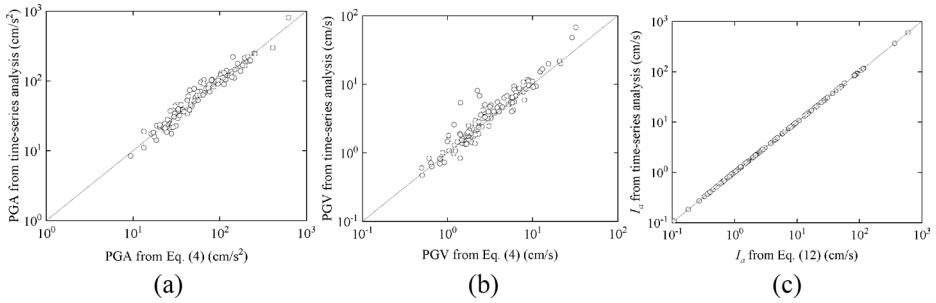

Fig. 4 Comparisons of results for (**a**) PGA, (**b**) PGV, and (**c**) I_a, calculated using Eqs. (4) or (12) and time-series analysis based on real seismic records

tive error across different periods being about 6%. The likely reason is that the rms duration D_{rms} model (Eq. (11)), used to modify the assumptions in RVT, is not sufficiently accurate for such cases. Additionally, the errors for V_{eq} and I_a are similar when using real seismic records and simulated time series. However, the errors for PSA, PGA, and PGV are lower when using simulated time series compared to those obtained from real seismic records.

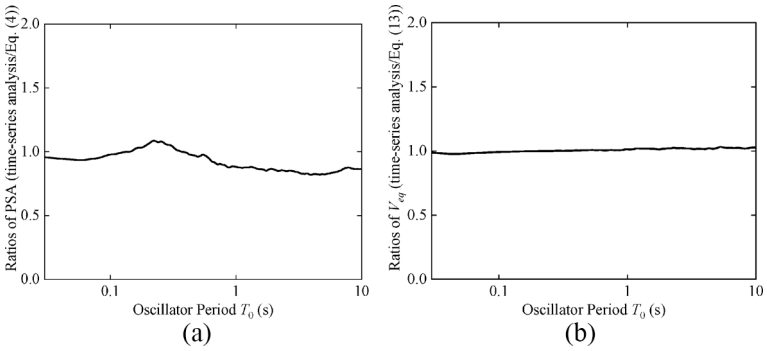

Fig. 5 Ratios of the average (**a**) PSA and (**b**) V_{eq} values obtained from time-series analysis to those from Eqs. (4) and (13) considering all real seismic records

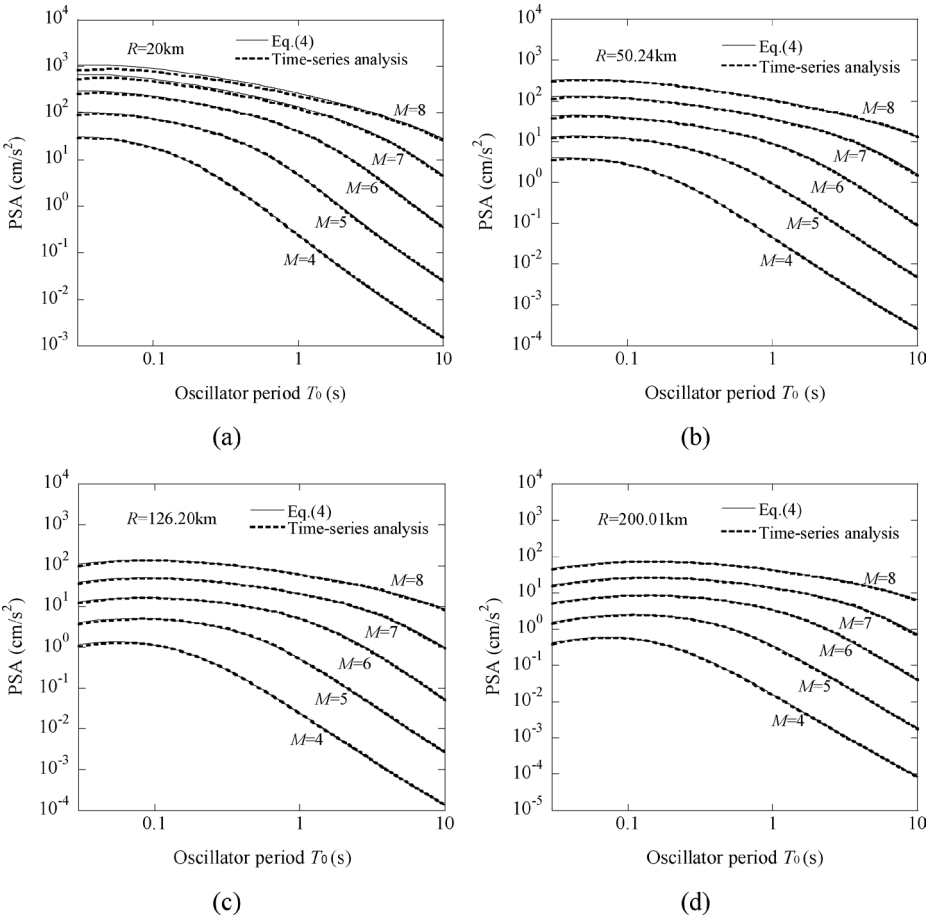

Fig. 6 Comparisons of PSA results calculated using Eq. (4) and time-series analysis based on a point-source FAS model for the cases of: (**a**) $R = 20$ km, (**b**) $R = 50.24$ km, (**c**) $R = 126.20$ km, and (**d**) $R = 200.01$ km

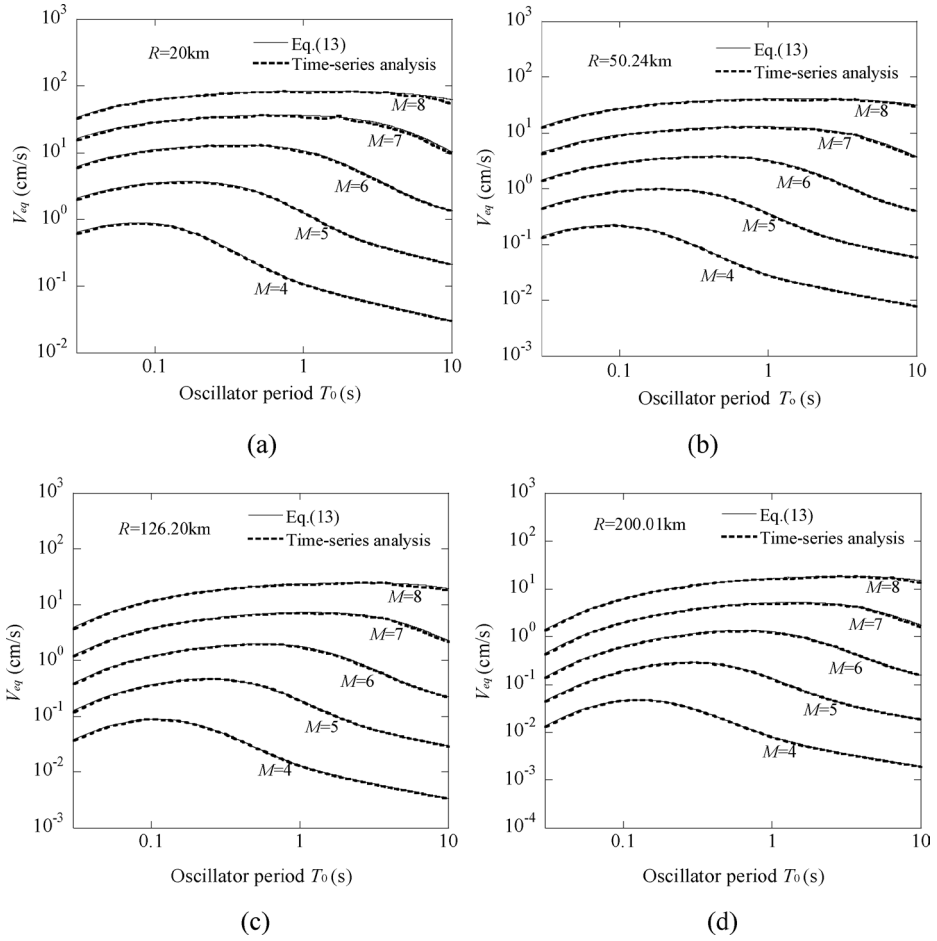

Fig. 7 Comparisons of V_{eq} results calculated using Eq. (13) and time-series analysis based on a point-source FAS model for the cases of: (**a**) $R=20$ km, (**b**) $R=50.24$ km, (**c**) $R=126.20$ km, and (**d**) $R=200.01$ km

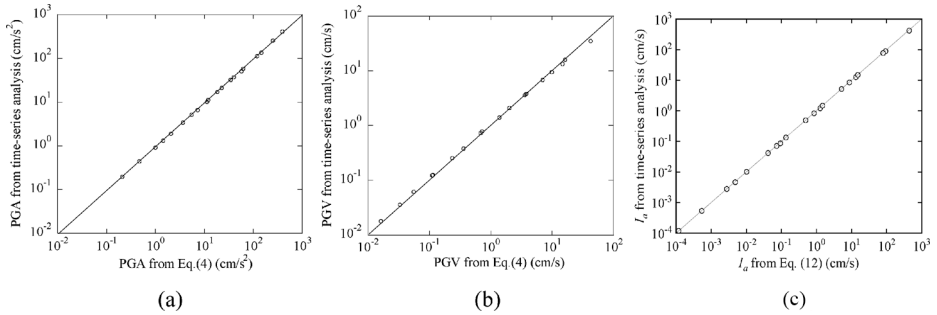

Fig. 8 Comparisons of results for (**a**) PGA, (**b**) PGV, and (**c**) I_a, calculated using Eqs. (4) or (12) and time-series analysis based on a point-source FAS model

Moreover, comparing the results for PGA, PGV, PSA, V_{eq}, and I_a obtained using the equations presented in Section 3, with those directly derived from the GMPEs of these intensity measures may also be necessary for accuracy investigation. However, this would require a central FAS GMPE, a duration model, and corresponding GMPEs for each intensity measure, all constructed based on the same ground-motion database to ensure consistency. This is because if the database used to develop the FAS GMPE and duration model differs from that used for the GMPEs of these intensity measures, their estimated results will differ, even if the equations presented in Section 3 are fully accurate. Since such a set of consistent GMPEs is currently unavailable, this comparison will need to be conducted in future studies.

4 Seismic hazard curves for multiple intensity measures

It is observed from Eq. (3) that calculating the exceedance probability or seismic hazard curves involves multiple integrals, which are generally difficult to solve theoretically. Therefore, it is common practice in the traditional PSHA framework to discretize the continuous distributions for M and R and to convert the integrals into discrete summations (Baker 2008). Each element within these discrete summations can be treated as an individual earthquake, characterized by magnitude, distance, focal parameters, etc. Since the natural logarithm of the IM for given a magnitude and a distance is typically considered to follow a normal distribution, the probability that IM exceeds a specified value $P(\mathrm{IM}>im|m, r)$ can be directly obtained using the CDF of the normal distribution. Ultimately, the exceedance probability $p_k(IM>im)$ can be obtained by summing that of each discrete earthquake.

However, employing such an approach to compute the exceedance probability $p_k(IM>im)$ within the proposed framework is not feasible. This is not only due to the additional integrals required to compute multiple intensity measures from FAS (Eqs. (4) – (14)), but more importantly, it is difficult to estimate $P(\mathrm{IM}>im|m, r)$ for these intensity measures directly from a given PDF of the FAS. This difficulty arises because the proposed framework relies exclusively on the GMPE for FAS and ground-motion duration model, instead of directly using GMPEs for PGA, PGV, PGD, PSA, V_{eq}, and I_a. Monte Carlo (MC) simulation can be used to address these challenges. Specifically, (1) firstly, generate enough samples for each random variable following given distributions; (2) then, estimate results of multiple intensity measures according to generated samples for each random variable using the equations in Section 3; (3) finally, calculate the exceedance probability $p_k(IM>im)$ by statistical analysis of all the obtained results. The accuracy of results by the MC simulation depends on the number of generated samples for each random variable, it increases with increasing the sample number. We attempted to calculate $p_k(IM>im)$ for PGA, PGV, PSA, I_a, and V_{eq} using 100,000 samples for each random variable, which is considered sufficient to obtain reliable results corresponding to exceedance probabilities greater than 0.001, covering most cases of interest in engineering (Zhao and Lu 2021). However, it costs about 2 hours for a single oscillator period considering a single source. The computation time also depends on the computer used in this study, which features a 12th Gen Intel Core i7-12,700 processor, 16GB of memory, and a 256GB NVMe SSD. If multiple sources and oscillator periods are considered as in real cases, the MC simulation may be prohibitively inefficient.

Therefore, a more efficient method, namely the moment method (Zhao and Ono 2001), is adopted in this paper to solve the calculation. The moment method calculates the exceedance probability $p_k(\mathrm{IM} > im)$ by two fundamental steps: (1) assume a distribution form for these intensity measures defined in terms of the first several statistical moments; and (2) estimate the first several statistical moments of these intensity measures according to the PDFs of the basic random variables including *M, R*, and residuals in the GMPE for FAS and ground-motion duration model.

The natural logarithm of intensity measures is assumed to follow a three-parameter distribution defined in terms of mean value, deviation and skewness (Zhao et al. 2001; Zhao and Lu 2021). The reason for using the three-parameter distribution is that it fits statistical data better, particularly for those with skewness, than traditional two-parameter distributions, e.g., normal and lognormal distributions. Figure 9 presents an example comparison of the three-parameter distribution and the normal distribution in fitting the distribution of $\ln V_{eq}$ (T_0=10 s) for seismic zone C, as discussed in Section 5 (details provided below). The CDF of the three-parameter distribution corresponding to $p_k(\ln(\mathrm{IM}) > \ln(im))$, $F_k(\ln(\mathrm{IM}))$, is expressed as,

$$F_k(ln(IM)) = \Phi\left[\frac{1}{\alpha_{3IM}}\left(\sqrt{9+\frac{1}{2}\alpha_{3IM}^2+6\alpha_{3IM}\frac{ln(IM)-\mu_{1IM}}{\sigma_{IM}}}-\sqrt{9-\frac{1}{2}\alpha_{3IM}^2}\right)\right] \tag{17}$$

where, μ_{1IM}, σ_{IM}, and α_{3IM} are the mean value, standard deviation, and skewness of the natural logarithm of the intensity measures. The standard deviation σ_{IM} and the skewness α_{3IM} can be estimated by the following equations:

$$\sigma_{IM}=\sqrt{\mu_{2IM}-\mu_{1IM}^2} \tag{18}$$

$$\alpha_{3IM}=\frac{\mu_{3IM}-3\mu_{2IM}\mu_{1IM}+2\mu_{1IM}^3}{\sigma_{IM}^3} \tag{19}$$

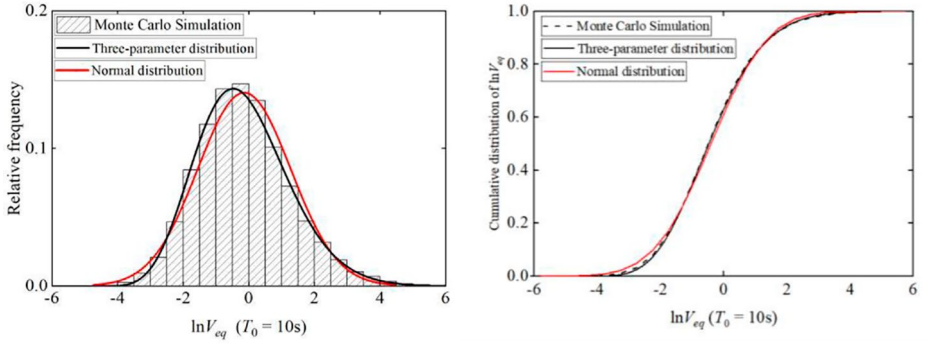

Fig. 9 Comparisons of the three-parameter distribution and the normal distribution in fitting the distribution of $\ln V_{eq}$ (T_0=10 s) for seismic zone C (Section 5)

where, μ_{1IM}, μ_{2IM}, and μ_{3IM} are the first-order, second-order, and three-order statistical moments of the natural logarithm of these intensity measures, respectively. It is noted that once the three statistical moments are determined, $F_k(\ln(\mathrm{IM}))$ and thus seismic hazard curves can be obtained. In theory, the *k*th-order statistical moment μ_{kIM} is expressed as,

$$\mu_{kIM} = E\left[ln(IM)^k\right] = \int_M \int_R \int_{R_{FAS}} \int_{R_D} ln(IM)^k f_M(m) f_R(r) f_{R_{FAS}}(r_{FAS}) f_{R_D}(r_D)\, dm dr dr_{FAS} dr_D \quad (20)$$

where R_{FAS} represents the residual in the GMPE for FAS, and R_D represents the residual in the ground-motion duration D_{gm} model. The residuals R_{FAS} and R_D refer to the misfit of a particular realization relative to the median predicted by the FAS GMPE and the D_{gm} model, respectively. For the estimation of I_a and V_{eq}, since D_{gm} is not used, the integral with respect to R_D and the associated PDF for R_D will not appear in Eq. (20).

It can be noted that Eq. (20) also contains complex multiple integrals. To simplify the calculation, the Latin hypercube sampling (LHS) simulation (McKay et al. 1979) was adopted to calculate the first three statistical moments. Unlike MC simulation, which relies on random sampling, LHS uses a stratified sampling strategy. This approach ensures that each segment of the input range is sampled, providing a more comprehensive and evenly distributed coverage of the input space. Therefore, adopting LHS simulation requires fewer samples and thus less calculation time while maintaining nearly the same accuracy as MC simulation.

Figure 10 presents the flowchart of the proposed framework for computing seismic hazard curves for multiple intensity measures. Firstly, samples for each random variable (including *M* and *R*) and the residuals (including R_{FAS} and R_D) are generated using LHS

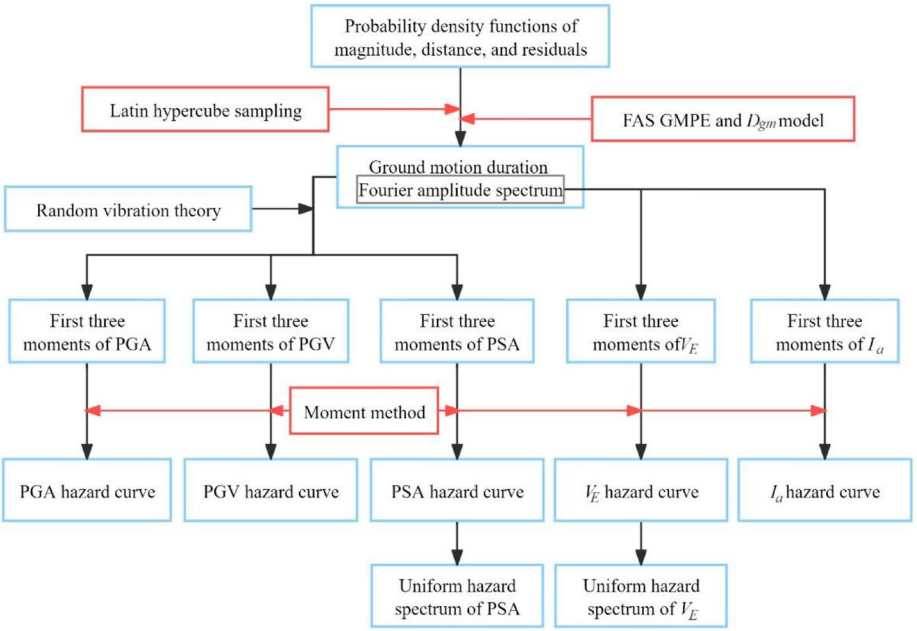

Fig. 10 Flowchart illustrating the proposed framework for computing hazard curves of multiple intensity measures

according to their PDFs. Then, the FAS and ground-motion duration D_{gm} are estimated for each set of samples based on the selected FAS GMPE and D_{gm} model. Next, multiple intensity measures are derived from the FAS and ground-motion duration D_{gm} according to Eqs. (4) – (14), and subsequently, the first three statistical moments for each intensity measure can be obtained through statistical analysis. Finally, the CDFs for each intensity measure are calculated using Eqs. (17) – (19). The exceedance probabilities and corresponding seismic hazard curves, considering all the earthquake sources, are then derived using Eqs. (1) and (2).

Additionally, applying the proposed framework allows for the consideration of epistemic uncertainties in a manner similar to the traditional approach. A logic tree scheme, employing multiple alternative GMPEs for FAS and duration D_{gm} models with assigned weights, can be used to address epistemic uncertainties. The calculation process simply involves repeating the procedure shown in Fig. 10 for each branch of the logic tree. However, whether the use of a logic tree scheme in the proposed framework will produce epistemic uncertainties consistent with those of the conventional approach may need to be systematically discussed in future studies

5 Numerical example

To demonstrate the efficiency and accuracy of the proposed framework, an example calculation was conducted in this section. This example considers three seismic zones, as shown in Fig. 11. The PDFs of the closest distance from the site to the surface projection of the rupture plane distance, R_{JB}, for the three seismic zones, are assumed to be Lognormal. The mean value of R_{JB}, the standard deviation of R_{JB}, and the mean annual rate for each seismic zone are presented in Table 1. The truncated exponential recurrence model is utilized as the PDF for magnitude, with the minimum threshold magnitude set as 6, and the maximum threshold magnitude set as 8. The statistical parameter θ is set as 2.6, and the time interval t is considered to be 50 years. In addition, the time-averaged shear wave velocity in the upper 30 m of the soil profile beneath the site, Vs_{30}(m/s), is considered to be 180 m/s.

In addition, the GMPE for FAS and ground-motion duration model developed by Bora et al. (2014) were adopted in the example calculation. The FAS GMPE is expressed as:

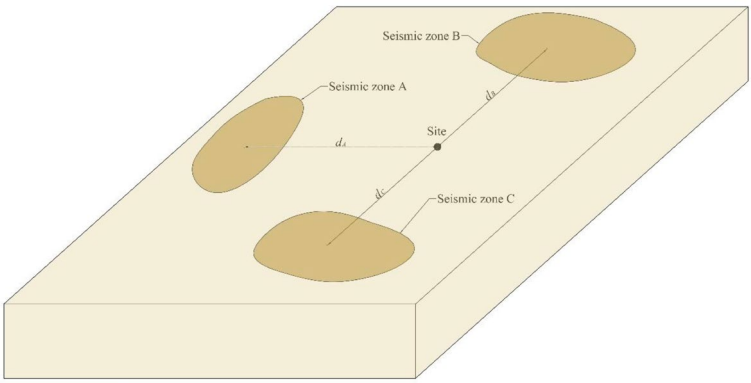

Fig. 11 Details of seismic zones utilized for numerical analyses

Table 1 Detail information of each seismic zone

Seismic zone	Mean value of R_{JB} (km)	Standard deviation of R_{JB} (km)	The mean annual rate
Seismic zone A	289.50	61.42	0.04
Seismic zone B	282.43	24.22	0.06
Seismic zone C	252.24	40.11	0.12

$$\begin{aligned} ln(Y(\omega)) &= c_0+c_1M+c_2M^2+(c_3+c_4M)ln(\sqrt{R_{JB}^2+c_5^2}) \\ &-c_6\sqrt{R_{JB}^2+c_5^2}+c_7ln(Vs_{30})+\eta+\varepsilon \end{aligned} \tag{21}$$

In this equation, $Y(\omega)$ is the geometric mean of FAS from both the horizontal components at circular frequency ω. In addition, $c_0 \sim c_7$ are regression coefficients for the FAS GMPE, η represents the between-event error, ε represents the within-event error, they were assumed to be normally distributed with zero means and standard deviation τ and φ respectively. The total standard deviation, σ, is calculated by $\sigma = \sqrt{\tau^2+\varphi^2}$. The values of the parameters $c_0 \sim c_7$, τ, φ, and σ were given in Table 2 of Bora et al. (2014).

The ground-motion duration D_{gm} model is expressed as:

$$ln(D_{gm}) = c_0+c_1M+(c_2+c_3M)ln(\sqrt{R_{JB}^2+c_4^2})+c_5ln(Vs_{30})+\eta+\varepsilon \tag{22}$$

where, D_{gm} (s) is the geometric mean of the duration estimated from the two horizontal components, and $c_0 \sim c_5$ are regression coefficients for the D_{gm} model. The values of the standard deviations τ and φ of the between-event error η and within-event error ε, as well as the total standard deviation σ in Eq. (22), were all provided in Table 1 of Bora et al. (2014).

Then, seismic hazard curves for PGA, PGV, PSA, I_a, and V_{eq} were calculated based on the proposed framework. 2,000 samples were generated for each random variable and residual based on the LHS. These results were then compared with those obtained from MC using 100,000 samples for each random variable. Representative comparisons are depicted in Figs. 12, 13 and 14. Figure 12 presents seismic hazard curves for PGA, PGV, and I_a. Figure 13 presents seismic hazard curves for PSA at different oscillator periods along with the corresponding uniform hazard spectra. Figure 14 presents seismic hazard curves for V_{eq} at different oscillator periods as well as the corresponding uniform hazard spectra.

It can be observed that the results of the proposed framework generally agree well with those of the MC simulation. Although errors increase as the exceedance probability decreases for some intensity measures (e.g., PGA, PGV, I_a, and PSA at T_0=0.1s), the relative error for most cases of interest in engineering (with exceedance probabilities less than 10^{-2} in 50 years) is less than 10%. Similarly, for the uniform hazard spectra of PSA, errors for oscillator periods around 1 s also increase as the exceedance probability decreases, but the average relative error across different periods remains within 5%. These errors are primarily associated with the sample size in the LHS, decreasing as the number of samples increases, but at the cost of increased computation time. In addition, the proposed framework requires only 1/50 of the calculation time compared to the MC simulation. The MC

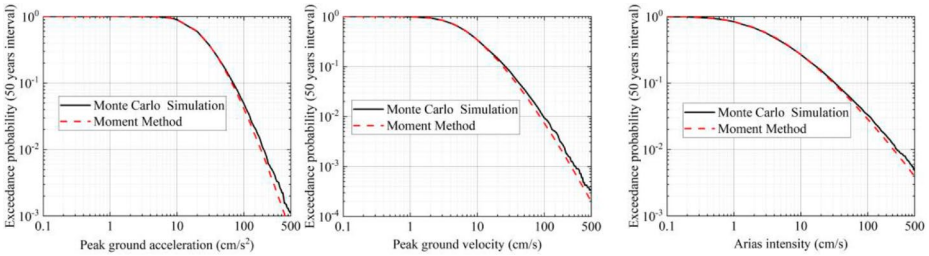

Fig. 12 Exceedance probabilities of (**a**) PGA, (**b**) PGV, and (**c**) I_a at 50 years intervals obtained using the proposed framework (2,000 samples) and MCS (100,000 samples)

simulation took approximately 6 hours to calculate the results in these figures, while the proposed framework required less than 10 minutes. In addition, it can be observed that the proposed framework can simultaneously provide seismic hazard curves for multiple intensity measures. From the discussion outlined above, it can be concluded that the proposed framework can efficiently estimate multiple intensity measures and provide their seismic hazard curves with relatively high accuracy.

Nevertheless, when adopting the proposed framework, it should be noted that, since the intensity measures are not directly estimated using their GMPEs but are instead transferred from FAS GMPEs and duration models, errors may be introduced into the PSHA results during this process. How to effectively address these errors in PSHA remains uncertain. Similarly, errors arising from the adopted LHS and moment method could also influence the results. These errors can be reduced by increasing the number of LHS samples, though this comes at the cost of increased computation time. Additionally, although the proposed framework can incorporate epistemic uncertainties using a logic tree scheme, whether it will produce epistemic uncertainty consistent with the conventional approach also remains unclear. These issues warrant further exploration in future studies.

6 Conclusions

This study proposed an efficient, physically reasonable, and internally consistent framework for probabilistically analyzing multiple intensity measures to derive their seismic hazard curves. Different from the traditional approach, this study exclusively adopts the GMPE of the FAS coupled with a ground-motion duration model, instead of directly using GMPEs for multiple intensity measures. Subsequently, multiple intensity measures are simultaneously estimated based on relationships between FAS with each intensity measure. Such that, the need to construct multiple GMPEs, as in the traditional approach, is circumvented. Additionally, deriving the desired intensity measures from a central GMPE ensures internal consistency among these intensity measures. Moreover, given that Fourier spectra are more closely related to the physics of wave propagation, the scaling of FAS in GMPEs is easier to constrain using seismological theory than the scaling of multiple intensity measures in GMPEs. Furthermore, the moment method, in conjunction with Latin hypercube sampling, is applied to calculate the exceedance probability for each intensity measure,

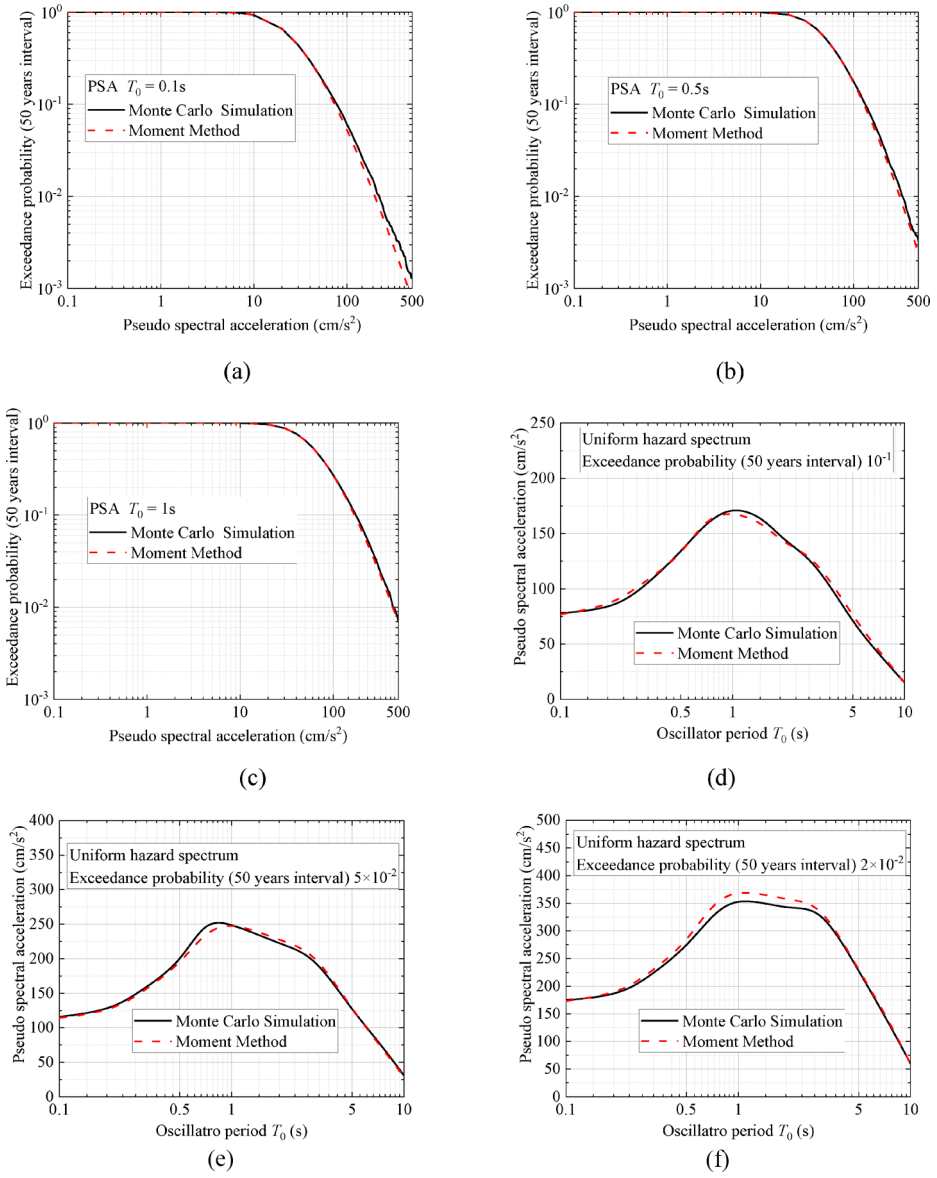

Fig. 13 Exceedance probabilities of PSA at 50 years intervals obtained using the proposed framework (2,000 samples) and MCS (100,000 samples), for cases of (**a**) T_0=0.1s, (**b**) T_0=0.5s, (**c**) T_0=1s. Additionally, uniform hazard spectra of PSA corresponding to exceedance probabilities of (**d**) 0.1, (**e**) 0.05, and (**f**) 0.02 at 50 years intervals, obtained using the proposed framework (2,000 samples) and MCS (100,000 samples)

thereby obtaining corresponding seismic hazard curves. The main conclusions of this study can be briefly summarized as follows:

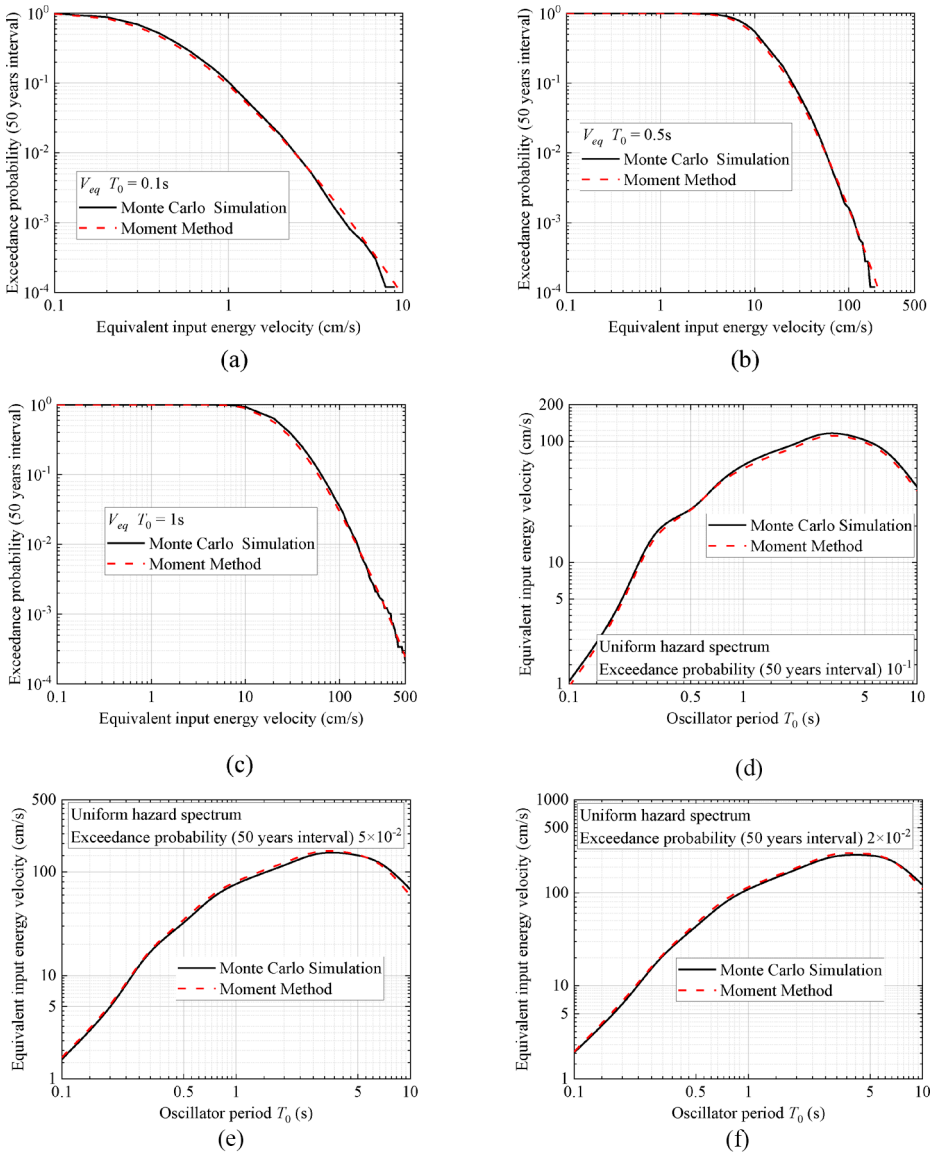

Fig. 14 Exceedance probabilities of V_{eq} at 50 years intervals obtained using the proposed framework (2,000 samples) and MCS (100,000 samples), for cases of (**a**) T_0=0.1s, (**b**) T_0=0.5s, (**c**) T_0=1s. Additionally, uniform hazard spectra of V_{eq} corresponding to exceedance probabilities of (d) 0.1, (**e**) 0.05, and (**f**) 0.02 at 50 years intervals, obtained using the proposed framework (2,000 samples) and MCS (100,000 samples)

(1) The accuracy of the approach for estimating multiple intensity measures from FAS was confirmed by comparing results of PGA, PGV, PSA, V_{eq}, and I_a with those from time-series analysis, based on a point-source FAS model and many real seismic records.

(2) An example calculation was conducted to demonstrate the efficiency and accuracy of the proposed framework. It was found that the proposed framework is highly efficient, requiring only 1/50 of the calculation time compared to the MC simulation, while still achieving a high level of accuracy comparable to that of the MC simulation.

Acknowledgments This work was supported by the Japan Society for the Promotion of Science (JSPS) KAKENHI (Grant No. 24K17336) as well as the National Natural Science Foundation of China (Grant No. 52278135), the authors are grateful for the financial supports. The authors are also grateful to Liutian Yu for help with the illustration of the figures in this paper.

Author contributions Haizhong Zhang: conceptualization, methodology, writing-original draft preparation, investigation. Yan-Gang Zhao: data curation, visualization, supervision. Rui Zhang: conceptualization, methodology, data curation, visualization. Hongjun Si: data curation, visualization, supervision

Funding The research leading to these results received fundings from the Japan Society for the Promotion of Science (JSPS) KAKENHI (Grant No. 24K17336) as well as the National Natural Science Foundation of China (Grant No. 52,278,135).

Data availability All data generated or analyzed during this study are included in this article.

Code availability Available upon request.

Declarations

Competing interests The authors have no competing interests to declare that are relevant to the content of this article.

References

AIJ (2015) Architectural Institute of Japan. Recommendations for loads on buildings 2015. in Japanese

AIR-Worldwide (2013) Study of impact and the insurance and economic cost of a major earthquake in British Columbia and Ontario/Québec. In: Commissioned by the Insurance Bureau of Canada. Boston

Alıcı FS, Sucuoğlu H (2016) Prediction of input energy spectrum: attenuation models and velocity spectrum scaling. Earthq Eng Struct D 45(13):2137–2161. https://doi.org/10.1002/eqe.2749

Alıcı FS, Sucuoğlu H (2018) Elastic and inelastic near-fault input energy spectra. Earthq Spectra 34(2):611–637. https://doi.org/10.1193/090817EQS175M

Allen TI, Griffin JD, Leonard M, Clark DJ, Ghasemi H (2020) The 2018 national seismic hazard assessment of Australia: quantifying hazard changes and model uncertainties. Earthq Spectra 36(1):5–43. https://doi.org/10.1177/8755293019900777

ASCE/SEI 7–22 (2022) Minimum design loads and associated criteria for buildings and other structures Published by the American society of civil engineers

Baker JW (2008). An introduction to probabilistic seismic hazard analysis (PSHA) version. 1(3):24–36

Bayless J, Abrahamson NA (2019) Summary of the BA18 ground-motion model for Fourier amplitude spectra for crustal earthquakes in California. Bull Seismol Soc Am 109(5):2088–2105. https://doi.org/10.1785/0120190077

Boore DM (1983) Stochastic simulation of high-frequency ground motions based on seismological models of the radiated spectra. Bull Seismol Soc Am 73(6A):1865–1894. https://doi.org/10.1785/BSSA07306A1865

Boore DM, Joyner WB (1984) A note on the use of random vibration theory to predict peak amplitudes of transient signals. Bull Seismol Soc Am 74(5):2035–2039. https://doi.org/10.1785/BSSA0740052035

Boore DM (2003) Simulation of ground motion using the stochastic method. Pure Appl Geophys 160(3):635–676. https://doi.org/10.1007/PL00012553

Boore DM (2005) SMSIM - Fortran programs for simulating ground motions from earthquakes: version 2.3 – a revision of OFR 96-80-A. Technical report United States Geological Survey, Reston, VA. https://doi.org/10.3133/ofr00509
Boore DM, Thompson EM (2015) Revisions to some parameters used in stochastic-method simulations of ground motion. Bull Seismol Soc Am 105(2A):1029–1041. https://doi.org/10.1785/0120140281
Bora SS, Scherbaum F, Kuehn N, Stafford P (2014) Fourier spectral- and duration models for the generation of response spectra adjustable to different source-, propagation-, and site conditions. Bull Earthq Eng 12(1):467–493. https://doi.org/10.1007/s10518-013-9482-z
Bora SS, Scherbaum F, Kuehn N, Stafford P (2016) On the relationship between Fourier and response spectra: implications for the adjustment of empirical ground-motion prediction equations (GMPEs). Bull Seismol Soc Am 106(3):1235–1253. https://doi.org/10.1785/0120150129
Building Standard Law (BSL) (2005) Notification no. 631 of the ministry of land, infrastructure, transport and tourism. Earthquake-Resistant Structural Calculation Based on Energy Balance, Tokyo, Japan
Chapman MC (1999) On the use of elastic input energy for seismic hazard analysis. Earthq Spectra 15(4):607–635. https://doi.org/10.1193/1.1586064
Cartwright DE, Longuet-Higgins MS (1956) The statistical distribution of the maxima of a random function. Proc Math Phys Eng Sci 237(1209):212–232. https://doi.org/10.1098/rspa.1956.0173
Cheng Y, Lucchini A, Mollaioli F (2014) Proposal of new ground-motion prediction equations for elastic input energy spectra. Earthq Struct 7(4):485–510. https://doi.org/10.12989/eas.2014.7.4.485
Cheng Y, Lucchini A, Mollaioli F (2020) Ground-motion prediction equations for constant-strength and constant-ductility input energy spectra. Bull Earthq Eng 18(1):37–55. https://doi.org/10.1007/s10518-019-00725-x
Chou CC, Uang CM (2000) Establishing absorbed energy spectra-an attenuation approach. Earthq Eng Struct D 29(10):1441–1455. https://doi.org/10.1002/1096-9845(200010)29:10%3C1441::AID-EQE967%3E3.0.CO;2-E
Davenport AG (1964) Note on the distribution of the largest value of a random function with application to gust loading. Pro Inst Civ Engrs 28(2):187–196. https://doi.org/10.1680/iicep.1964.10112
Douglas J (2024) Ground motion prediction equations 1964–2023. http://www.gmpe.org.uk/
Kuwamura H, Galambos TV ((1989)) Earthquake load for structural reliability. J Struct Eng 115(6):1446–1462. https://doi.org/10.1061/(ASCE)0733-9445(1989)115:6(1446)
Lavrentiadis G, Abrahamson NA (2023) A non-ergodic spectral acceleration ground motion model for California developed with random vibration theory. B Earthq Eng 21:5265–5291. https://doi.org/10.1007/s10518-023-01689-9
Liu L, Pezeshk S (1999) An improvement on the estimation of pseudoresponse spectral velocity using RVT method. Bull Seismol Soc Am 89(5):1384–1389. https://doi.org/10.1785/BSSA0890051384
McKay MD, Beckman RJ, Conover WJ (1979) A comparison of three methods for selecting values of input variables in the analysis of output from a computer Code. Technometrics 21(2):239–245. https://doi.org/10.1080/00401706.1979.10489755
Nigam N, Jennings P (1969) Calculation of response spectra from strong-motion earthquake records. Bull Seismol Soc Am 59(2):909–922. https://doi.org/10.1785/BSSA0590020909
National Earthquake Hazards Reduction Program (NEHRP) (2000) Recommended Provisions for Seismic Regulations for New Buildings and Other Structures. Federal Emergency Management Agency, Washington, D.C
Ordaz M, Huerta B, Reinoso E (2003) Exact computation of input-energy spectra from Fourier amplitude spectra. Earthq Eng Struct D 32(4):597–605. https://doi.org/10.1002/eqe.240
Reed JW, Kassawara RP (1990) A criterion for determining exceedance of the operating basis earthquake. Nucl Eng Des 123(2–3):387–396. https://doi.org/10.1016/0029-5493(90)90259-Z
Stafford PJ, Rodriguez-Marek A, Edwards B, Kruiver PP, Bommer JJ (2017) Scenario dependence of linear site-effect factors for short-period response spectral ordinates. Bull Seismol Soc Am 107(6):2859–2872. https://doi.org/10.1785/0120170084
Standards Australia (2007) Structural design actions, Part 4: earthquake actions in Australia (Standards Australia AS 1170.4–2007). Sydney, NSW, Australia
Travasarou T, Bray JB, Abrahamson A (2003) Empirical attenuation relationship for Arias Intensity. Earthq Eng Struct D 32(7):1133–1155. https://doi.org/10.1002/eqe.270
Tselentis GA, Danciu L (2010) Probabilistic seismic hazard assessment in Greece– part 1: engineering ground motion parameters. Nat Hazards Earth Syst Sci 10(1):25–39. https://doi.org/10.5194/nhess-10-25-2010
Tselentis GA, Danciu L, Sokos E (2010) Probabilistic seismic hazard assessment in Greece - Part 2: acceleration response spectra and elastic input energy spectra. Nat Hazards Earth Syst Sci 10(1):41–49. https://doi.org/10.5194/nhess-10-41-2010
Vanmarcke EH (1975) On the distribution of the first-passage time for normal stationary random processes. J Appl Mech 42(1):215–220. https://doi.org/10.1115/1.3423521

Walker GR (2008) Earthquake insurance: an Australian perspective. Aust J Struct Eng 8(1):39–48. https://doi.org/10.1080/13287982.2008.11464985
Wang XY, Rathje EM (2016) Influence of peak factors on site amplification from random vibration theory based site-response analysis. Bull Seismol Soc Am 106(4):1733–1746. https://doi.org/10.1785/0120150328
Zhang HZ, Zhao YG (2020) Damping modification factor based on random vibration theory using a source-based ground-motion model. Soil Dyn Earthq Eng 136:106225. https://doi.org/10.1016/j.soildyn.2020.106225
Zhang HZ, Zhao YG (2021a) Effects of earthquake magnitude, distance, and site conditions on spectral and pseudospectral velocity relationship. Bull Seismol Soc Am 111(6):3160–3174. https://doi.org/10.1785/012021015
Zhang HZ, Zhao YG (2021b) Analytical model for response spectral ratio considering the effect of earthquake scenarios. B Earthq Eng 19(1). https://doi.org/10.1007/s10518-021-01166-1
Zhang HZ, Zhao YG (2022) Damping modification factor of acceleration response spectrum considering seismological effects. J Earthq Eng 26(16):8359–8382. https://doi.org/10.1080/13632469.2021.1991521
Zhang HZ, Zhao YG, Ge FW, Fang YC, Ochiai T (2023a) Estimation of input energy spectrum from pseudo-velocity response spectrum incorporating the influences of magnitude, distance, and site conditions. Eng Struct 274:115165. https://doi.org/10.1016/j.engstruct.2022.115165
Zhang HZ, Zhao YG, Ochiai T, Fang YC (2023b) Relationship between SDOF-input-energy and Fourier amplitude spectral amplification ratios. Bull Seismol Soc Am 113(3):1230–1247. https://doi.org/10.1785/0120220154
Zhang R, Zhao YG, Zhang HZ (2024a) An efficient method for probability prediction of peak ground acceleration using Fourier amplitude spectral model. J Earthq Eng 28(6):1495–1511. https://doi.org/10.1080/13632469.2023.2241549
Zhang HZ, Zhang R, Zhao YG (2024b) Novel Approach for Energy-Spectrum-Based Probabilistic Seismic Hazard Analysis in Regions with Limited Strong Earthquake Data. Earthq Spectra (Accepted)
Zhao YG, Lu ZH (2021) Structural reliability: approaches from perspectives of statistical moments. Wiley, HobokenAmerica
Zhao YG, Ono T (2001) Moments methods for structural reliability. Struct Saf 23(1):47–75. https://doi.org/10.1016/S0167-4730(00)00027-8
Zhao YG, Ono T, Idota H, Hirano T (2001) A three-parameter distribution used for structural reliability evaluation. J Struct Constr Eng AIJ 66(546):31–38. https://doi.org/10.3130/aijs.66.31_6
Zhao YG, Zhang R, Zhang HZ (2023) Probabilistic prediction of ground-motion intensity for regions lacking strong ground-motion records. Soil Dyn Earthq Eng 165:107706. https://doi.org/10.1016/j.soildyn.2022.107706

Authors and Affiliations

Haizhong Zhang[1] · Yan-Gang Zhao[2] · Rui Zhang[3] · Hongjun Si[4]

✉ Rui Zhang
zhangrui@qlnu.edu.cn

[1] Eco-Science Course, Faculty of Agriculture, Yamagata University, 1-23, Wakaba-machi, Tsuruoka-shi, Yamagata 997-8555, Japan

[2] Key Laboratory of Urban Security and Disaster Engineering of Ministry of Education, Beijing University of Technology, Beijing 100124, China

[3] School of Geography and Tourism, Qilu Normal University, Jinan 250200, China

[4] Seismological Research Institute Inc., Tokyo, Japan